Odoni DI, Tamayo-Ramos JA, Sloothaak J, van Heck RGA, Martins dos Santos VAP, de Graaff LH, Suarez-Diez M, Schaap PJ. 2017. Comparative proteomics of *Rhizopus delemar* ATCC 20344 unravels the role of amino acid catabolism in fumarate accumulation. PeerJ 5:e3133 https://doi.org/10.7717/peerj.3133

Comparative proteomics of *Rhizopus delemar* ATCC 20344 unravels the role of amino acid catabolism in fumarate accumulation

Dorett I Odoni [1], **Juan A Tamayo-Ramos** [1], **Jasper Sloothaak** [1], **Ruben G A van Heck** [1], **Vitor A P Martins dos Santos** [1,2], **Leo H de Graaff** [1], **Maria Suarez-Diez** [1], **Peter J Schaap** [Corresp. 1]

[1] Laboratory of Systems and Synthetic Biology, Wageningen University and Research, Wageningen, The Netherlands

[2] LifeGlimmer GmBH, Berlin, Germany

Corresponding Author: Peter J Schaap
Email address: peter.schaap@wur.nl

The filamentous fungus *Rhizopus delemar* naturally accumulates relatively high amounts of fumarate. Although the culture conditions that increase fumarate yields are well established, the network underlying the accumulation of fumarate is not yet fully understood. We set out to increase the knowledge about fumarate accumulation in *R. delemar*. To this end, we combined a transcriptomics and proteomics approach to identify key metabolic pathways involved in fumarate production in *R. delemar*, and propose that a substantial part of the fumarate accumulated in *R. delemar* during nitrogen starvation results from the urea cycle due to amino acid catabolism.

Comparative proteomics of *Rhizopus delemar* ATCC 20344 unravels the role of amino acid catabolism in fumarate accumulation

Dorett I Odoni[1+], Juan A Tamayo-Ramos[1+^], Jasper Sloothaak[1], Ruben G A van Heck[1], Vitor A P Martins dos Santos[1], Leo H de Graaff[†], Maria Suarez-Diez[1] and Peter J Schaap[1]

[1] Laboratory of System and Synthetic Biology, Wageningen University and Research, Stippeneng 4, 6708 WE Wageningen, the Netherlands

[^] Current address: International Research Centre in Critical Raw Materials-ICCRAM, University of Burgos, Plaza Misael Banuelos s/n, 09001 Burgos, Spain

[+]Equal contributions

†Deceased 16 October 2016

Corresponding author:

Peter J Schaap[1]

Email address:

PJS: peter.schaap@wur.nl

PeerJ Preprints | https://doi.org/10.7287/peerj.preprints.2742v1 | CC BY 4.0 Open Access | rec: 23 Jan 2017, publ: 23 Jan 2017

Abstract

The filamentous fungus *Rhizopus delemar* naturally accumulates relatively high amounts of fumarate. Although the culture conditions that increase fumarate yields are well established, the network underlying the accumulation of fumarate is not yet fully understood. We set out to increase the knowledge about fumarate accumulation in *R. delemar*. To this end, we combined a transcriptomics and proteomics approach to identify key metabolic pathways involved in fumarate production in *R. delemar*, and propose that a substantial part of the fumarate accumulated in *R. delemar* during nitrogen starvation results from the urea cycle due to amino acid catabolism.

Introduction

Fumarate, a dicarboxylic acid, is an important building block chemical for a number of high-value chemicals and materials. Amongst the microorganisms identified to be natural fumarate producers, the filamentous fungus *Rhizopus delemar* has the highest product yields [1]. The most important factor influencing fumarate production in *R. delemar* is a high carbon:nitrogen ratio; extracellular fumarate accumulation happens after the growth phase, and especially when the nitrogen in the medium has been depleted [2,3]. The choice of nitrogen source has been reported to influence the final fumarate yield [1,4,5], but so far no consensus on these influences has been reached. Another important factor influencing fumarate production in *R. delemar* is oxygen availability [1,6]. Under fumarate producing conditions, *R. delemar* forms ethanol and other undesired fermentation by-products [7], directing carbon away from fumarate (Fig. 1). Higher oxygen levels limit the amount of ethanol produced, and thus lead to higher fumarate yields. Fumarate production by fermentation has been extensively reviewed [8,9].

PeerJ Preprints | https://doi.org/10.7287/peerj.preprints.2742v1 | CC BY 4.0 Open Access | rec: 23 Jan 2017, publ: 23 Jan 2017

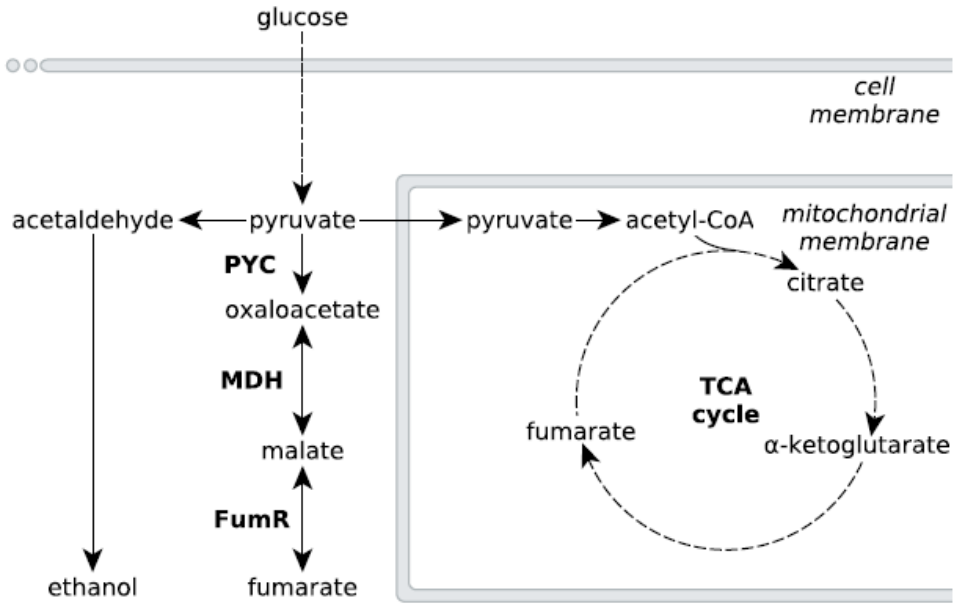

Figure 1. Metabolic pathways involved in fumarate metabolism in *R. delemar*.
Metabolic flux of *R. delemar* is predominantly directed towards fumarate (under aerobic conditions) or ethanol (under anaerobic conditions). The enzymes of the reductive TCA cycle are indicated in the scheme: PYC = pyruvate carboxylase, MDH = L-malate dehydrogenase and FumR = fumarase.

Although the culture conditions that increase fumarate accumulation in *R. delemar* are well established, natural product titers still cannot compete with chemical fumarate synthesis. To increase the amount of fumarate produced, *R. delemar* has been genetically modified [10–12], but the occurrence of an ancestral whole-genome duplication as well as more recent gene-duplication events complicate the genetic engineering of *R. delemar* [13]. A more promising approach for biological fumarate production would thus be rewiring the metabolism of a genetically more amenable cell-factory, based on *R. delemar* fumarate synthesis pathways.

Metabolic engineering approaches to increase fumarate production in microbial cell-factories that do not naturally accumulate high amounts of fumarate would greatly benefit from an in-

PeerJ Preprints | https://doi.org/10.7287/peerj.preprints.2742v1 | CC BY 4.0 Open Access | rec: 23 Jan 2017, publ: 23 Jan 2017

66 depth understanding of the underlying metabolic pathways that affect the accumulation of
67 fumarate in the natural fumarate producer *R. delemar*, as well as possible causes for this
68 accumulation. Fumarate can be found as an intermediate in various different metabolic
69 subsystems, and a number of pathways have been investigated for fumarate production in
70 several microbial cell-factories such as *Saccharomyces cerevisiae*, *Torulopsis glabrata*,
71 *Scheffersomyces stipitis* and *Escherichia coli* [14–22]. Despite the large number of pathways
72 leading to fumarate, the current consensus is that the reductive route of the TCA cycle in the
73 cytosol is responsible for fumarate accumulation in *R. delemar* [23–27]. The reductive TCA
74 cycle comprises pyruvate carboxylase (PYC), L-malate dehydrogenase (MDH) and fumarase
75 (FumR), in which pyruvate is consecutively converted to oxaloacetate, L-malate and fumarate
76 (Fig. 1).
77
78 A controversial aspect of this pathway model is FumR. While overexpression of *pyc* and *mdh*
79 gave the expected increase of fumarate in *R. delemar* and *Saccharomyces cerevisiae* [11,20],
80 overexpression of *fumR* in *R. delemar* as well as the introduction of *fumR* in *S. cerevisiae* and
81 *A. niger* was reported to result in more L-malate rather than the accumulation of fumarate
82 [12,20,28]. There has been debate about the role of FumR in fumarate accumulation,
83 discussed by Meussen *et al.* [10]. In summary, the reaction kinetics of FumR favour the
84 conversion of fumarate to L-malate rather than the reverse direction, and FumR activity of
85 acid-producing mycelium is completely blocked in the presence of 2 mM fumarate
86 (unpublished data, cited by [3,10]). This suggests the presence of an alternative pathway that
87 is responsible for fumarate accumulation in *R. delemar*.
88
89 In this study, we aim to provide a holistic overview of the pathways involved in fumarate
90 accumulation in the natural fumarate producer *R. delemar*. To this end, we cultured the *R.*

PeerJ Preprints | https://doi.org/10.7287/peerj.preprints.2742v1 | CC BY 4.0 Open Access | rec: 23 Jan 2017, publ: 23 Jan 2017

delemar strain ATCC 20344 under nitrogen starvation conditions, and varied oxygen availability to induce high (aerobic) and low (anaerobic) fumarate production. Combining transcriptomic and proteomic data obtained from the two conditions, we revealed the relationship between nitrogen metabolism and fumarate accumulation in *R. delemar*, mediated by the urea cycle.

Materials and Methods

Strains, media and culture conditions

We selected the *R. delemar* strain ATCC 20344 (a kind gift from Adrie J.J. Straathof, Delft University of Technology) to study fumarate production. Note that *R. delemar* is more commonly known as *R. oryzae* (also *Rhizopus nigricans* and *Rhizopus arrhizus*) [29]. Depending on the organic acid produced when grown on D-glucose, it is divided into two phylogenetically distinct types: type I strains, which produce primarily L-lactate, and type II strains, which produce mainly fumarate and L-malate [30]. Complete medium agar plates containing 0.3% (w/v) yeast extract, 0.3% (w/v) malt extract, 0.3% (w/v) peptone, 2% (w/v) glycerol, and 2% (w/v) agar were used to generate spores. Mycelial biomass was produced using pre-culture medium containing 1% (w/v) D-glucose, 0.21% (w/v) urea, 0.06% (w/v) KH_2PO_4, 0.05% (w/v) $MgSO_4 \cdot 7H_2O$ and 0.0018% (w/v) $ZnSO_4 \cdot 7H_2O$. Approximately 10^6 spores/mL were inoculated in 1L Erlenmeyer flasks containing 500 mL of pre-culture medium and cultivations were carried out at 35°C and 250 rpm for 24 hours. The mycelium obtained was washed with demineralized water and transferred (≈ 25 g of wet biomass) to production medium, which contained 10% (w/v) D-glucose, 0.06% (w/v) KH_2PO_4, 0.05% (w/v) $MgSO_4 \cdot 7H_2O$, 0.0018% (w/v) $ZnSO_4 \cdot 7H_2O$, and 1% (w/v) $CaCO_3$ (used as a neutralizing agent). Batch fermentations were performed at 35°C and 600 rpm in 2.5 L fermentors (Applikon, Schiedam, the Netherlands), with a working volume of 1.75 L.

PeerJ Preprints | https://doi.org/10.7287/peerj.preprints.2742v1 | CC BY 4.0 Open Access | rec: 23 Jan 2017, publ: 23 Jan 2017

Antifoam 204 was added to each fermentor (85 µL). The fermentation medium was aerated with 1.0 L/L min, either with filtered air or N_2 gas.

Metabolite analysis using HPLC

Extracellular metabolite concentrations were determined by high-performance liquid chromatography (HPLC). A Thermo Accela HPLC, equipped with a Shodex KC-811 column, and coupled to a refractive index detector (Spectrasystem RI-150, sample frequency 5.00032Hz) and a UV–VIS detector (Spectrasytem UV1000, λ = 210 nm), was used. Separations were performed by isocratic elution with 0.01 N H_2SO_4 at a flow rate of 0.8 mL/min. Crotonic acid (6 mM) was used as an internal standard.

RNA isolation and quality control

Frozen mycelium (≈ 100 mg) of *R. delemar* ATCC 20344 was submerged in 1 mL of Trizol reagent in a 2 mL tube, prefilled with a mix of glass beads with the following diameters: 1 mm (0.25 g), 0.1 mm (0.37 g), 5 mm (1 bead). Mycelium samples were disrupted using a FastPrep-24 Instrument (MP). After disruption, 200 µL of chloroform were added and the mix was homogenated for 10 seconds. The mix was poured into phase-lock gel tubes (2 mL), and centrifuged at maximum speed in a table-top centrifuge. The RNA present in the water phase was purified using the RNeasy Mini Kit (Qiagen), following the manufacturer's instructions. RNA integrity was assessed with an Experion system (Bio-Rad), and only high quality samples (RIN value ≥ 8) were selected for whole transcriptome shotgun sequencing.

RNA sequencing and quality check

Illumina RNA sequencing (RNA seq) using the Casava pipeline version 1.8.2 and subsequent quality analysis of the FASTQ sequence reads was performed by BaseClear (Leiden, the

PeerJ Preprints | https://doi.org/10.7287/peerj.preprints.2742v1 | CC BY 4.0 Open Access | rec: 23 Jan 2017, publ: 23 Jan 2017

Netherlands). The number of reads obtained was 20'539'199 for the aerobic and 24'519'028 for the anaerobic condition, with an average quality score (Phred) of 37.59 and 37.91, respectively. The raw data has been submitted to the EMBL-EBI database, and can be found under the accession number PRJEB14210.

RNA seq data processing

The RNA seq reads were filtered using SortMeRNA v1.9 [31], cutadapt v1.2.1 [32] and PRINSEQ v0.20.2 [33]. *De novo* assembly of the reads that passed the quality filtering was performed using the IDBA-UD assembler v1.1 [34]. Read mapping and transcript coverage calculations were performed using Bowtie2 v 2.2.2 [35] and BEDTools [36]. Note that in contrast to the proteomics analysis, which was performed on both biological replicates, only one biological replicate per condition was sent for RNA sequencing. The average nucleotide coverage is thus an indication of the transcript levels of a given transcript the time of sampling, not the average of two biological replicates.

Preparation of cell free extracts for proteomic analysis

R. delemar ATCC 20344 mycelium samples (2-3 g, press-dried), were washed with an ice-cold 20 mM HEPES buffer pH 7.6, containing 150 mM NaCl, and resuspended in the same solution containing 1% (v/v) protease inhibitor cocktail for yeast and fungi (Sigma). Mycelium suspensions were immediately disrupted using a French press (8000 psi). Cell free extracts were centrifuged for 5 min at low speed (500 g), in order to remove unbroken cells and pellet debris. The remaining supernantants were further processed for LC-MS/MS analysis.

PeerJ Preprints | https://doi.org/10.7287/peerj.preprints.2742v1 | CC BY 4.0 Open Access | rec: 23 Jan 2017, publ: 23 Jan 2017

Sample preparation for LC-MS/MS

The protein content of the *R. delemar* ATCC 20344 cell free extracts was determined using the BCA protein assay (Thermo Fisher). Membrane-bound proteins were solubilised by mixing volumes of each sample, containing 25 µg of protein, with equal volumes of a 2x solution of 20 mM HEPES pH 7.6**,** containing 1 M 6-aminocaproic acid and 10 g L^{-1} of n-dodecyl-beta-D-maltoside. Cell free extract-detergent mixes were incubated in a thermoblock for 1 h at 20°C and vigorous stirring (1000 rpm). Afterwards, samples were sonicated in a water bath for 15 min, and finally they were centrifuged at 22000 g, in a benchtop centrifuge, for 30 min. Obtained supernatants were subsequently concentrated using MMicrocon YM-10 columns (cutoff, 10 kDa; Millipore, Eschborn, Germany).

Samples from each biological replicate and culture condition were loaded into a 12% SDS-polyacrylamide gel, which was run until the loaded samples entered the gel. The gel was stained according to the manufacturer's instructions using Page Blue staining (Fermentas) and rinsed with ultrapure water. Each sample-gel lane was cut into one slice (approx. 1 cm^2), carefully sliced into smaller pieces of about 1 mm^3 and transferred into microcentrifuge tubes. Samples were destained and equilibrated through three washing steps using the following solutions: 50 mM ammonium bicarbonate (ABC) (incubated 5 min), ABC/acetonitrile (1:1, v/v) (incubated 5 min) and neat acetonitrile (incubated 5 min). These washing steps were repeated two times. The gel samples were then swelled in 10 mM dithiothreitol (DTT) for 20 min at 56°C to reduce protein disulfide bonds. Subsequently, the DTT solutions were removed and samples were alkylated with 50 mM 2-chloroacetamide in ABC, for 20 min, at room temperature, in the dark. The 2-chloroacetamide solutions were removed, and samples were again washed twice with: neat acetonitrile (incubated 5 min), ABC (incubated 5 min) and neat acetonitrile (incubated 5 min). Approximately 150 µL of digestion buffer, containing sequencing grade modified trypsin (12.5 ng/µL) (Promega) in ABC, was added to each

PeerJ Preprints | https://doi.org/10.7287/peerj.preprints.2742v1 | CC BY 4.0 Open Access | rec: 23 Jan 2017, publ: 23 Jan 2017

sample, making sure that all gel pieces were kept wet during digestion (adding, if necessary, additional ABC solution). Protein samples were digested overnight at 37°C. Peptide digestion products were extracted by adding 50 µL of 2% trifluoroacetic acid (TFA), followed by an incubation step in a thermoblock for 20 min, at room temperature and vigorous stirring (1400 rpm). Gel pieces were then subjected to 20 s sonication in a water bath, centrifuged and supernatants were transferred to new tubes. The peptide extraction step was then repeated once by washing the gel pieces with buffer B (80% acetonitrile, 0.1% formic acid) followed by the mentioned incubation and sonication steps. Supernatants from both extractions were pooled and samples were placed in a vacuum centrifuge for acetonitrile evaporation util 20-40 µL were left. Finally, samples were acidified by addition of TFA (1:1, v/v) and peptide clean-up procedure, prior to LC-MS/MS analysis, was performed using the "STop And Go Extraction" procedure as described before [37].

Mass spectrometric measurements and proteomic data analysis

LC-MS/MS analysis was performed at the Radboud Proteomics Centre as described previously [38]. Measurements were performed by nanoflow reversed-phase C18 liquid chromatography (EASY nLC, Thermo Scientific) coupled online to a 7 Tesla linear ion trap Fourier-Transform ion cyclotron resonance mass spectrometer (LTQ FT Ultra, Thermo Scientific). The LC-MS/MS spectra obtained were identified and quantified using the maxQuant software [39]. The peptides were mapped against the *in silico* proteomes of *R. delemar* ATCC 20344 (obtained from the transcriptomics experiment) and RA 99-880 (obtained from Genbank, Project ID: 13066 [13]) with the default settings, described in [40]. Only proteins with 2 or more unique peptide hits were considered for further analysis. The mass spectrometry proteomics data have been deposited to the ProteomeXchange Consortium via the PRIDE [41] partner repository with the dataset identifier PXD004600.

PeerJ Preprints | https://doi.org/10.7287/peerj.preprints.2742v1 | CC BY 4.0 Open Access | rec: 23 Jan 2017, publ: 23 Jan 2017

Metabolic pathway enrichment analysis

Metabolic enzymes were annotated using PRIAM [42], and subsequently assigned to KEGG pathways [43,44]. Enrichment analysis of differentially expressed pathways was performed using the hypergeometric test implementation ("phyper") of the R software environment [45]. We used the identified proteins that could be mapped to a KEGG pathway as the universe (with size N = 277). Note that the terms "differentially expressed" and "overexpressed" refer to differences in relative protein abundances, and denote a fold-change of 1.5 and 2 as lenient and stringent thresholds.

Results and Discussion

Fumarate and ethanol production of ATCC 20344 grown under aerobic and anaerobic conditions

We chose to work with *R. delemar* ATCC 20344, henceforth referred to as ATCC 20344, for its ability to produce fumarate in high quantities [46]. ATCC 20344 was grown in batch fermentations under nitrogen starved conditions. The fumarate production rate was controlled by either supplying filtered air to the culture medium (aerobic condition), or restricting the amount of oxygen by flushing the system with N_2 (anaerobic condition). D-glucose, fumarate and ethanol concentrations in the supernatant were measured *via* High Performance Liquid Chromatography (HPLC) to determine the time point with the largest difference in fumarate yield. The HPLC analysis showed comparable D-glucose consumption rates in the two conditions (Fig. 2), with an average of 0.15 ± 0.03 g/h and 0.11 ± 0.03 g/h for the aerobic and anaerobic condition, respectively. Fumarate production was higher in the aerobic condition, whereas in the anaerobic condition ethanol production prevailed. Note that Lin *et al.* showed that *Rhizopus spp.* grow very poorly under absolute anaerobic conditions, but that most of the tested strains grew "quite well" under microaerobic conditions [47]. The use of silicone

PeerJ Preprints | https://doi.org/10.7287/peerj.preprints.2742v1 | CC BY 4.0 Open Access | rec: 23 Jan 2017, publ: 23 Jan 2017

241 tubing on our fermentors, which are slightly oxygen permeable even when flushed with pure
242 nitrogen gas [48], allowed ATCC 20344 to grow at a normal rate, while keeping fumarate
243 production to a minimum. However, the amount of oxygen entering through the silicone
244 tubing was below the detection limit of the probes measuring dissolved oxygen in the
245 fermentors, and we refer to the two conditions as "aerobic" and "anaerobic" rather than
246 "aerobic" and "microaerobic".
247

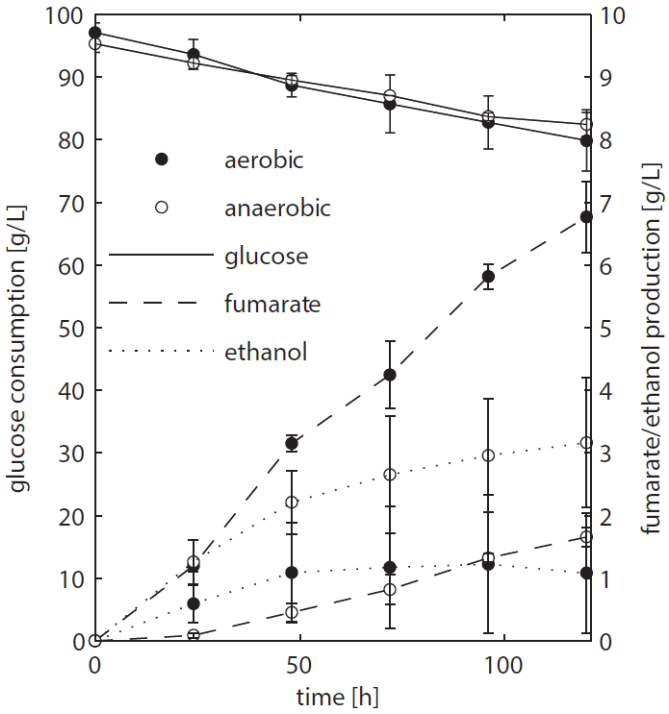

248

249 **Figure 2. HPLC analysis of fermentation broth of *R. delemar* ATCC 20344 grown under**
250 **aerobic and anaerobic conditions.**
251 Total D-glucose consumption and fumarate and ethanol production of *R. delemar* ATCC
252 20344. The measurement points show the average of two biological replicates.
253

254 The fumarate yields (gram per gram substrate D-glucose consumed) are summarised in Table
255 1. The maximum fumarate yield (0.41 ± 0.06 g/g) in the aerobic condition was observed after
256 96 hours of fermentation. A comparable yield (0.35 ± 0.05 g/g) was already observed after 24

PeerJ Preprints | https://doi.org/10.7287/peerj.preprints.2742v1 | CC BY 4.0 Open Access | rec: 23 Jan 2017, publ: 23 Jan 2017

hours of fermentation. In contrast, the fumarate yield in the anaerobic condition increased continuously at a slow pace, being highest after 120 hours of fermentation (0.13 ± 0.02 g/g). Thus, the largest difference in fumarate yield between the two conditions was observed at the start of the experiment, and we chose t = 24 h as the time point for the transcriptome and proteome analyses.

Table 1. Fumarate yields of ATCC 20344 grown under aerobic and anaerobic conditions.

Time [h]	Fumarate yield ± sd [g/g D-glucose]	
	aerobic	anaerobic
24	0.349 ± 0.055	0.029 ± 0.015
48	0.375 ± 0.001	0.077 ± 0.015
72	0.380 ± 0.055	0.098 ± 0.012
96	0.411 ± 0.063	0.115 ± 0.014
120	0.397 ± 0.044	0.132 ± 0.022

Transcriptome and proteome of ATCC 20344 under high and low fumarate producing conditions

Enzyme activities, and thus metabolism, are affected by various factors such as post-translational modifications, allosteric control, and substrate availability. Metabolic fluxes can therefore not be inferred directly from protein abundances. Nevertheless, contrasting enzyme abundance levels between the high and low fumarate producing condition (ATCC 20344 snapshot proteomes) indicate differences in the metabolic state of ATCC 20344 at the time point of sampling. To determine differential protein abundances *via* LC-MS/MS, a reference proteome database is required for peptide mass fingerprinting. To date, *R. delemar* RA 99-880, henceforth referred to as RA 99-880, is the only fully sequenced *R. delemar* strain of

PeerJ Preprints | https://doi.org/10.7287/peerj.preprints.2742v1 | CC BY 4.0 Open Access | rec: 23 Jan 2017, publ: 23 Jan 2017

276 which also the proteome is publicly available [13]. However, if the RA 99-880 reference
277 proteome is used as only reference database, conservative amino acid substitutions in ATCC
278 20344 will reduce the sensitivity, as protein identification relies on an exact peptide mass. To
279 provide a complete database of the metabolic potential as well as an overview of the
280 metabolic state of ATCC 20344 under high and low fumarate producing conditions, we
281 combined transcriptomic and proteomic data of ATCC 20344 grown under high and low
282 fumarate producing conditions. The transcriptome was used to construct a database of the
283 ATCC 20344 *in silico* proteome, and the relative protein abundances were obtained by
284 mapping the peptides from the snapshot proteomes against both the ATCC 20344 and RA 99-
285 880 *in silico* proteomes, the latter to account for possible errors in the *de novo* transcript
286 assembly. The experimental setup is outlined in Fig. 3.
287

PeerJ Preprints | https://doi.org/10.7287/peerj.preprints.2742v1 | CC BY 4.0 Open Access | rec: 23 Jan 2017, publ: 23 Jan 2017

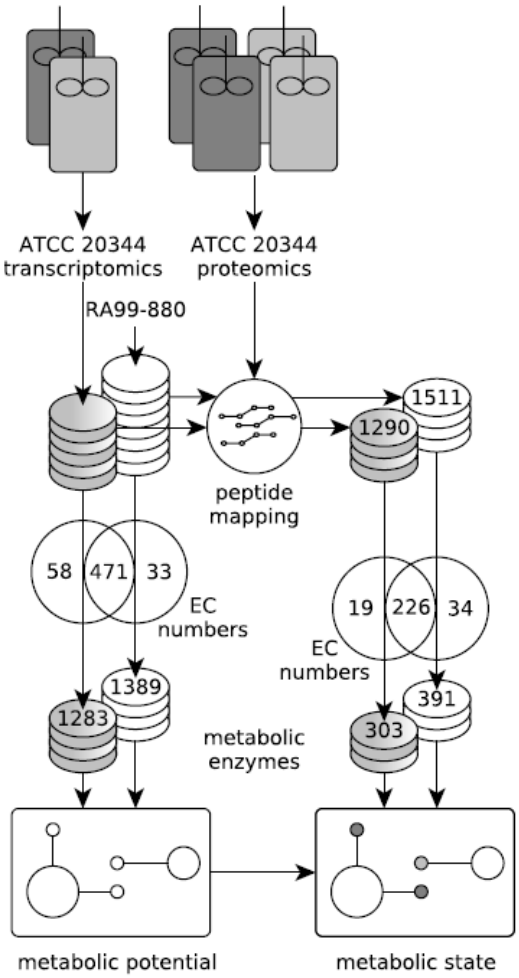

Figure 3. Experimental setup.

Workflow to establish the metabolic potential and metabolic state of ATCC 20344 grown under high and low fumarate producing conditions. The metabolic enzymes predicted in the ATCC 20344 and RA 99-880 *in silico* proteomes provide a map of the metabolic potential, while the metabolic enzymes identified in the proteomics experiment were used to determine the metabolic state of ATCC 20344 under high and low fumarate producing conditions.

The RNA seq reads obtained from the aerobic and anaerobic conditions were combined into one dataset, and assembled *de novo*, resulting in 13'531 contigs (File S1). EC numbers were assigned to the six-frame translation products of the *de novo* contigs, as well as to the RA 99-880 reference proteome (File S2). In ATCC 20344, we predicted 1283 metabolic enzymes,

PeerJ Preprints | https://doi.org/10.7287/peerj.preprints.2742v1 | CC BY 4.0 Open Access | rec: 23 Jan 2017, publ: 23 Jan 2017

covering 529 EC numbers. In RA 99-880, we predicted 1389 metabolic enzymes, covering 504 EC numbers. The metabolic enzymes were mapped to KEGG pathway maps [43,44] in order to obtain a rough estimate of the metabolic potential of *R. delemar*.

The proteins obtained from the aerobic and anaerobic conditions were subjected to a shotgun proteomics analysis. A total of 1290 and 1511 proteins were identified in the ATCC 20344 and RA 99-880 proteomes, respectively. Roughly one third of the identified proteins comprised metabolic enzymes. A list of all EC numbers predicted in the ATCC 20344 and RA 99-880 *in silico* proteomes, as well as the relative protein abundances and average nucleotide coverages of the proteins and transcripts identified in the experimental conditions, can be found in Table S3. The protein pathway coverage (number of ECs per pathway covered by proteins with the predicted function in ATCC 20344 and RA 99-880) is given in Table S4.

Metabolic pathway enrichment analysis

To determine which pathways play an important role in fumarate accumulation in ATCC 20344, we obtained a list of enzymatic proteins that directly consume or produce fumarate according to the KEGG database [43,44], and analysed their presence and abundance in the ATCC 20344 high and low fumarate producing conditions (Table 2). In addition, we performed pathway enrichment analysis of differentially expressed enzymes (Table 3, Table S4).

Table 2. List of enzymes involved in fumarate metabolism with their respective protein abundances under high and low fumarate producing conditions.

EC number	Consensus protein identifier[a]	Relative protein abundance ± sd [%]		Log_2FC aerobic/anaerobic	Enzyme name
		aerobic	anaerobic		

PeerJ Preprints | https://doi.org/10.7287/peerj.preprints.2742v1 | CC BY 4.0 Open Access | rec: 23 Jan 2017, publ: 23 Jan 2017

4.2.1.2	Rd_01690	1.51 ± 0.16	0.66 ± 0.06	1.21	fumarate hydratase (fumarase, FumR)
4.3.2.1	Rd_00962	0.09 ± 0.01	0.06 ± 0.02	0.60	argininosuccinate lyase (ASL)
1.3.98.1	Rd_00873	0.04 ± 4e-3	0.01 ± 2e-3	1.34	dihydroorotate dehydrogenase
3.7.1.2	Rd_01207	0.03 ± 3e-3	0.00	-	fumarylacetoacetase
1.3.5.1	Rd_01783	0.01 ± 2e-3	0.00	-	succinate dehydrogenase
4.3.2.2	Rd_00964	5e-3 ± 7e-4	0.01 ± 8e-7	-1.59	adenylosuccinate lyase

[a]Identifiers refer to IDs in Table S3. Note that, where possible, ATCC 20344 enzymes were prioritised. In this case, all enzymes were identified in the ATCC 20344 proteome.

Table 3. Metabolic pathway enrichment analysis.

Pathway	# ECs in reference pathway	# proteins (ECs) identified	Differentially expressed		Overexpressed (aerobic)			
			# proteins (1.5-fold)	p-value	# proteins (1.5-fold)	p-value	# proteins (2-fold)	p-value
Alanine, aspartate and glutamate metabolism	50	16 (12)	15	0.040	10	0.102	7	0.264
Arginine biosynthesis	32	14 (12)	13	0.070	10	0.033	5	0.534
beta-Alanine metabolism	37	11 (8)	9	0.389	9	0.011	9	0.001
Citrate cycle (TCA cycle)	25	19 (15)	14	0.589	10	0.292	9	0.143
Glycolysis / Gluconeogenesis	49	31 (19)	19	0.957	10	0.946	9	0.777
Oxidative phosphorylation	11	20 (8)	16	0.327	14	0.014	9	0.189
Pyrimidine	65	13 (11)	11	0.267	9	0.056	6	0.243

PeerJ Preprints | https://doi.org/10.7287/peerj.preprints.2742v1 | CC BY 4.0 Open Access | rec: 23 Jan 2017, publ: 23 Jan 2017

metabolism								
Pyruvate metabolism	68	23 (15)	17	0.565	11	0.433	11	0.102
Valine, leucine and isoleucine degradation	38	14 (10)	11	0.446	8	0.230	8	0.055

327

328 We found that, amongst the enzymes which interact directly with fumarate and were
329 identified in the ATCC 20344 snapshot proteomes, FumR (EC 4.2.1.2), is the most highly
330 abundant enzyme, both under high and low fumarate producing conditions (Table 2).
331 Although there is no clear enrichment of the TCA cycle enzymes among the differentially
332 expressed metabolic proteins (Table 3), the three enzymes of the reductive TCA cycle, PYC
333 (EC 6.4.1.1), MDH (EC 1.1.1.37), and FumR (EC 4.2.1.2), are all overexpressed in the high
334 fumarate producing condition (Table S3).

335

336 The second most highly abundant protein related to fumarate metabolism is argininosuccinate
337 lyase (ASL) (EC 4.3.2.1). ASL is a urea cycle enzyme involved in arginine biosynthesis. The
338 arginine biosynthesis pathway showed a significant number of differentially expressed
339 proteins (Table 3), and we found that the enzymes comprising the urea cycle are
340 overexpressed in the high fumarate producing condition (Table 4). This suggests that in
341 ATCC 20344, the urea cycle plays an important role in fumarate accumulation. Most
342 interestingly, ASL and FUM constitute a crucial link between carbon and nitrogen
343 metabolism by connecting the TCA- and urea cycles (also referred to as “Krebs bicycle”).

344

PeerJ Preprints | https://doi.org/10.7287/peerj.preprints.2742v1 | CC BY 4.0 Open Access | rec: 23 Jan 2017, publ: 23 Jan 2017

Table 4. Urea cycle enzymes with their respective protein abundances under high and low fumarate producing conditions.

EC number	Consensus protein identifier[a] (ref)	Relative protein abundance ± sd [%]		Log_2FC aerobic/anaerobic	Enzyme name
		aerobic	anaerobic		
2.1.3.3	Rd_01058 (A)	0.03 ± 0.01	0.02 ± 8e-3	0.51	ornithine carbamoyltransferase (OTC)
6.3.4.5	Rd_01708 (R)	0.86 ± 0.07	0.57 ± 0.05	0.59	argininosuccinate synthase (ASS)
6.3.4.5	Rd_01709 (R)	0.00	0.04 ± 0.02	-	argininosuccinate synthase (ASS)
4.3.2.1	Rd_00962 (A)	0.09 ± 0.01	0.06 ± 0.02	0.60	argininosuccinate lyase (ASL)
3.5.3.1	Rd_00988 (R)	0.13 ± 0.02	0.07 ± 0.01	0.97	arginase (ARG)
3.5.3.1	Rd_00989 (R)	0.19 ± 0.02	0.11 ± 0.03	0.76	arginase (ARG)

[a]Identifiers refer to IDs in Table S3. Note that, where possible, ATCC 20344 enzymes were prioritised. Letters in brackets refer to the reference proteome, with A = ATCC 20344 and R = RA 99-880.

The observed protein abundances for FumR and ASL offer an explanation for the importance of a high carbon:nitrogen ratio for fumarate accumulation in *Rhizopus spp*. In humans, starvation induces a net breakdown of stored energy sources, starting with fatty acids and, when exposed to prolonged starving conditions, proteins from muscle tissue. The degradation of protein, or amino acids, results in the liberation of ammonia, which is then carried to the urea cycle as L-glutamate. In the urea cycle, the L-glutamate is converted to urea, which is subsequently excreted. Based on the significant enrichment scores of pathways involved in

PeerJ Preprints | https://doi.org/10.7287/peerj.preprints.2742v1 | CC BY 4.0 Open Access | rec: 23 Jan 2017, publ: 23 Jan 2017

amino acid metabolism (Table 3), we propose that the nitrogen starvation, induced by the transfer of ATCC 20344 from growth- to production medium, triggers a similar switch in metabolism, and amino acid catabolism starts to occur. The resulting fluxes through the urea cycle yield an excess of fumarate (Fig. 4).

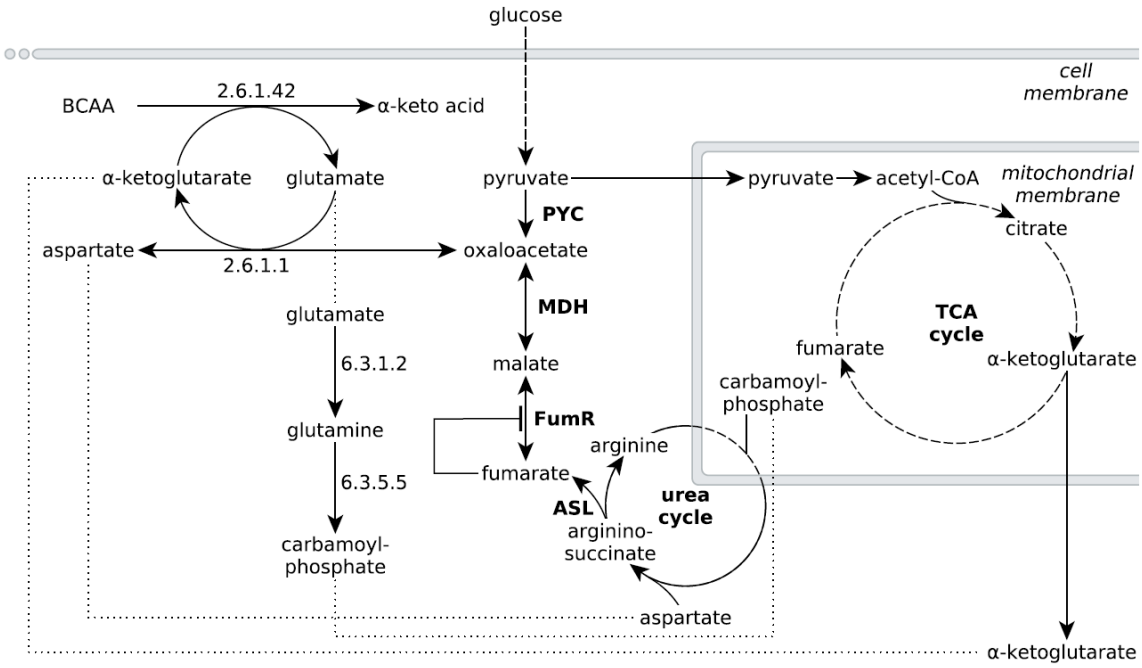

Figure 4. Extended network of metabolic pathways involved in fumarate metabolism in *R. delemar*.

The extended model of fumarate accumulation reconstructed from the ATCC 20344 snapshot proteomes under high and low fumarate producing conditions takes the formation of fumarate *via* the urea cycle into account.

Specifically, the pathway for the degradation of the branched-chain amino acids (BCAA) valine, leucine and isoleucine shows a significant number of overexpressed enzymes in high fumarate producing condition. BCAA catabolism is initiated by BCAA aminotransferase (EC 2.6.1.42), which catalyses the transfer of an amino group from any of the three BCAAs to α-ketoglutarate, yielding L-glutamate and the respective α-keto acid as products (Fig. 4). Under

PeerJ Preprints | https://doi.org/10.7287/peerj.preprints.2742v1 | CC BY 4.0 Open Access | rec: 23 Jan 2017, publ: 23 Jan 2017

starvation conditions in which both the nitrogen and carbon source in the culture medium are limited, the carbon skeletons of the deaminated amino acids can be used to replenish acetyl-CoA (from leucine), or the TCA cycle intermediate succinyl-CoA (from valine) or both of these metabolites (from isoleucine), and thereby, ultimately, to generate energy for growth. Under conditions of excess carbon and limited nitrogen, however, it is unlikely that amino acid catabolism is driven by energy demand of the organism. More importantly, it is crucial for *R. delemar* grown under nitrogen depleted conditions to decouple carbon catabolism from cell proliferation, as there is little nitrogen available for *de novo* protein biosynthesis.

One way to decouple carbon catabolism from biomass formation is by reducing the amount of ATP generated. Under aerobic growth conditions, ATP is generated *via* oxidative phosphorylation. Under anaerobic conditions, *R. delemar* generates ATP *via* ethanol fermentation (Fig. 1). Another option for ATP generation is alternative respiration, mediated by the key enzyme alternative oxidase (AOX). AOX diverts the electrons passing through the electron transport chain in the mitochondria at the ubiquinone pool and transfers them directly to oxygen, thereby bypassing the oxidative phosphorylation complexes III and IV, resulting in an overall lower ATP yield. Gu *et al*. found that the activity of AOX is positively correlated with fumarate production in *R. delemar* [49]. In contrast, we identified AOX (Rd_00967 (A)) only in the snapshot proteome of the anaerobic condition. The transcriptomics measurements further underpin our proteomics results, since *aox* was overexpressed (> 4-fold) in the anaerobic condition (Table S3). This might seem counterintuitive at first, since the expression of *aox* is generally regarded as a means of dealing with increased oxidative stress. However, the electron flow through AOX has been found to be inversely proportional to nitrogen availability in various different plant systems [50]. The increase of AOX under nitrogen limited conditions and the resulting decrease of the respiratory ATP yield have been

PeerJ Preprints | https://doi.org/10.7287/peerj.preprints.2742v1 | CC BY 4.0 Open Access | rec: 23 Jan 2017, publ: 23 Jan 2017

associated with a deliberately reduced efficiency in converting carbon to biomass; by using the non-energy conserving AOX, the "redundant" carbohydrate can be metabolised without being coupled to growth.

Another way of decoupling carbon catabolism from energy generation, and thereby cell proliferation, is channelling the products from amino acid degradation to the mitochondria for mitochondrial protein synthesis, and thereby away from cytosolic protein synthesis; a mechanism suggested to take place under nitrogen starvation conditions in human cells, irrespective of the D-glucose availability [51]. In this, amino acid catabolism is the first step to adapt to nitrogen limiting conditions, and we propose that, in a similar mechanism, the urea cycle plays a key role for the accumulation of fumarate in *R. delemar*. This is supported by the work of Chen *et al.*, who showed that, from a range of selected enzymes, overexpressing ASL, while keeping the expression of adenylosuccinate lyase low, resulted in the highest fumarate titer in *Torulopsis glabrata* [14].

Conclusions

The accumulation of fumarate in the natural fumarate producer *R. delemar* has been mostly attributed to the consecutive conversion of pyruvate to oxaloacetate, L-malate and fumarate by cytosolic enzymes of the reductive TCA cycle. In addition, our proteomics data have revealed that the nitrogen-limitation under fumarate producing conditions induces amino acid catabolism, which leads to an increased flux through the urea cycle. Our comparative proteomics analysis of high and low fumarate producing conditions in *R. delemar* ATCC 20344 has thus resulted in a novel holistic view on fumarate production that expands the knowledge on fumarate production in this fungus.

PeerJ Preprints | https://doi.org/10.7287/peerj.preprints.2742v1 | CC BY 4.0 Open Access | rec: 23 Jan 2017, publ: 23 Jan 2017

Acknowledgements

We would like to thank Sybe Hartmans, Michael Volpers and Brendan Ryback for critically reading and commenting on draft versions of the manuscript. In addition, we would like to thank Bastian Hornung for valuable input for the RNA seq data analysis, Ruud Weusthuis for valuable feedback on general aspects of this manuscript, and Tom Schonewille and Merlijn van Gaal for their contribution in the experimental part of this work.

References

1. Foster JW, Waksman SA. The Production of Fumaric Acid by Molds Belonging to the Genus *Rhizopus*. J Am Chem Soc. American Chemical Society; 1939;61: 127–135.
2. Magnuson J, Lasure L. Organic acid production by filamentous fungi. Adv fungal Biotechnol Ind Agric Med. 2004; 307–340.
3. Goldberg I, Rokem JS, Pines O. Organic acids: old metabolites, new themes. J Chem Technol Biotechnol. 2006;81: 1601–1611.
4. Rhodes R a, Moyer a J, Smith ML, Kelley SE. Production of fumaric acid by *Rhizopus arrhizus*. Appl Microbiol. 1959;7: 74–80.
5. Z.Y. Zhang, B. Jin JMK. Production of lactic acid and byproducts from waste potato starch by *Rhizopus arrhizus* : role of nitrogen sources. World J Microbiol Biotechnol. 2007;23: 229–236.
6. J. W. Foster, S.F. Carson, D.S Anthony, J.B. Davis, W.E. Jefferson MVL. Aerobic formation of fumaric acid in the mold *Rhizopus nigricans*: Synthesis by direct C2 condensation. Proc Natl Acad Sci. 1949;35.
7. Wright BE, Longacre A, Reimers J. Models of metabolism in *Rhizopus oryzae*. J Theor Biol. 1996;182: 453–7.
8. Straathof AJJ, van Gulik WM. Production of fumaric acid by fermentation. Subcell Biochem. 2012;64: 225–40.
9. Roa Engel CA, Straathof AJJ, Zijlmans TW, van Gulik WM, van der Wielen LAM. Fumaric acid production by fermentation. Appl Microbiol Biotechnol. 2008;78: 379–89.
10. Meussen BJ, de Graaff LH, Sanders JPM, Weusthuis RA. Metabolic engineering of *Rhizopus oryzae* for the production of platform chemicals. Appl Microbiol Biotechnol. 2012;94: 875–86.
11. Zhang B, Skory CD, Yang S-T. Metabolic engineering of *Rhizopus oryzae*: effects of overexpressing pyc and pepc genes on fumaric acid biosynthesis from glucose. Metab Eng. 2012;14: 512–20.
12. Zhang B, Yang S-T. Metabolic engineering of *Rhizopus oryzae*: Effects of overexpressing *fumR* gene on cell growth and fumaric acid biosynthesis from glucose. Process Biochem. 2012;47: 2159–2165.
13. Ma L-J, Ibrahim AS, Skory C, Grabherr MG, Burger G, Butler M, et al. Genomic analysis of the basal lineage fungus *Rhizopus oryzae* reveals a whole-genome duplication. PLoS Genet. 2009;5: e1000549.
14. Chen X, Wu J, Song W, Zhang L, Wang H, Liu L. Fumaric acid production by *Torulopsis glabrata*: engineering the urea cycle and the purine nucleotide cycle. Biotechnol Bioeng. 2015;112: 156–67.

15. Li N, Zhang B, Wang Z, Tang Y-J, Chen T, Zhao X. Engineering *Escherichia coli* for fumaric acid production from glycerol. Bioresour Technol. 2014;174: 81–7.
16. Song CW, Kim DI, Choi S, Jang JW, Lee SY. Metabolic engineering of *Escherichia coli* for the production of fumaric acid. Biotechnol Bioeng. 2013;110: 2025–34.
17. Wei L, Liu J, Qi H, Wen J. Engineering *Scheffersomyces stipitis* for fumaric acid production from xylose. Bioresour Technol. 2015;187: 246–54.
18. Xu G, Chen X, Liu L, Jiang L. Fumaric acid production in *Saccharomyces cerevisiae* by simultaneous use of oxidative and reductive routes. Bioresour Technol. 2013;148: 91–6.
19. Xu G, Liu L, Chen J. Reconstruction of cytosolic fumaric acid biosynthetic pathways in *Saccharomyces cerevisiae*. Microb Cell Fact. BioMed Central; 2012;11: 24.
20. Xu G, Zou W, Chen X, Xu N, Liu L, Chen J. Fumaric acid production in *Saccharomyces cerevisiae* by *in silico* aided metabolic engineering. PLoS One. Public Library of Science; 2012;7: e52086.
21. Zhang T, Wang Z, Deng L, Tan T, Wang F, Yan Y. Pull-in urea cycle for the production of fumaric acid in *Escherichia coli*. Appl Microbiol Biotechnol. 2015;99: 5033–44.
22. Chen X, Zhu P, Liu L. Modular optimization of multi-gene pathways for fumarate production. Metab Eng. 2016;33: 76–85.
23. Romano AH, Bright MM, Scott WE. Mechanism of fumaric acid accumulation in *Rhizopus nigricans*. J Bacteriol. 1967;93: 600–4.
24. Overman SA, Roman H. Pyruvate carboxylase of *Rhizopus nigricans* and its role in fumaric acid production. Biochem Biophys Res Commun. 1969;37: 457–463.
25. Osmani S A, Scrutton MC. The sub-cellular localisation and regulatory properties of pyruvate carboxylase from *Rhizopus arrhizus*. Eur J Biochem. 1985;147: 119–28.
26. Kenealy W, Zaady E, du Preez JC, Stieglitz B, Goldberg I. Biochemical Aspects of Fumaric Acid Accumulation by *Rhizopus arrhizus*. Appl Environ Microbiol. 1986;52: 128–33.
27. Peleg Y, Battat E, Scrutton M, Goldberg I. Isoenzyme pattern and subcellular localisation of enzymes involved in fumaric acid accumulation by *Rhizopus oryzae*. Appl Microbiol Biotechnol. Springer-Verlag; 1989;32: 334–339.
28. de Jongh WA, Nielsen J. Enhanced citrate production through gene insertion in *Aspergillus niger*. Metab Eng. 2008;10: 87–96.
29. Abe A, Oda Y, Asano K, Sone T. *Rhizopus delemar* is the proper name for *Rhizopus oryzae* fumaric-malic acid producers. Mycologia. 2007;99: 714–22.
30. Abe A, Sone T, Sujaya IN, Saito K, Oda Y, Asano K, et al. rDNA ITS sequence of *Rhizopus oryzae*: its application to classification and identification of lactic acid producers. Biosci Biotechnol Biochem. Japan Society for Bioscience, Biotechnology, and Agrochemistry; 2003;67: 1725–31.
31. Kopylova E, Noé L, Touzet H. SortMeRNA: fast and accurate filtering of ribosomal RNAs in metatranscriptomic data. Bioinformatics. 2012;28: 3211–7.
32. Martin M. Cutadapt removes adapter sequences from high-throughput sequencing reads. EMBnet.journal. 2011. pp. 10–12.
33. Schmieder R, Edwards R. Quality control and preprocessing of metagenomic datasets. Bioinformatics. 2011;27: 863–4.
34. Peng Y, Leung HCM, Yiu SM, Chin FYL. IDBA-UD: a *de novo* assembler for single-cell and metagenomic sequencing data with highly uneven depth. Bioinformatics. 2012;28: 1420–8.
35. Langmead B, Salzberg SL. Fast gapped-read alignment with Bowtie 2. Nat Methods. 2012;9: 357–9.

PeerJ Preprints | https://doi.org/10.7287/peerj.preprints.2742v1 | CC BY 4.0 Open Access | rec: 23 Jan 2017, publ: 23 Jan 2017

36. Quinlan AR, Hall IM. BEDTools: a flexible suite of utilities for comparing genomic features. Bioinformatics. 2010;26: 841–2.
37. Rappsilber J, Ishihama Y, Mann M. Stop and Go Extraction Tips for Matrix-Assisted Laser Desorption/Ionization, Nanoelectrospray, and LC/MS Sample Pretreatment in Proteomics. Anal Chem. American Chemical Society; 2003;75: 663–670.
38. Rajala N, Hensen F, Wessels HJCT, Ives D, Gloerich J, Spelbrink JN. Whole cell formaldehyde cross-linking simplifies purification of mitochondrial nucleoids and associated proteins involved in mitochondrial gene expression. PLoS One. Public Library of Science; 2015;10: e0116726.
39. Cox J, Mann M. MaxQuant enables high peptide identification rates, individualized p.p.b.-range mass accuracies and proteome-wide protein quantification. Nat Biotechnol. 2008;26: 1367–72.
40. Sloothaak J, Odoni DI, de Graaff LH, Martins Dos Santos VAP, Schaap PJ, Tamayo-Ramos JA. *Aspergillus niger* membrane-associated proteome analysis for the identification of glucose transporters. Biotechnol Biofuels. 2015;8: 150.
41. Vizcaíno JA, Csordas A, Del-Toro N, Dianes JA, Griss J, Lavidas I, et al. 2016 update of the PRIDE database and its related tools. Nucleic Acids Res. Oxford University Press; 2016;44: D447–D456.
42. Claudel-Renard C, Chevalet C, Faraut T, Kahn D. Enzyme-specific profiles for genome annotation: PRIAM. Nucleic Acids Res. 2003;31: 6633–9.
43. Kanehisa M, Goto S. KEGG: kyoto encyclopedia of genes and genomes. Nucleic Acids Res. 2000;28: 27–30.
44. Kanehisa M, Sato Y, Kawashima M, Furumichi M, Tanabe M. KEGG as a reference resource for gene and protein annotation. Nucleic Acids Res. 2015;44: D457-62.
45. R Core T. R: A language and environment for statistical computing. R Foundation for Statistical Computing, Vienna, Austria.; 2014.
46. Cao N, Du J, Gong CS, Tsao GT. Simultaneous Production and Recovery of Fumaric Acid from Immobilized *Rhizopus oryzae* with a Rotary Biofilm Contactor and an Adsorption Column. Appl Environ Microbiol. 1996;62.
47. Lin MS, Wang HH. Anaerobic growth and oxygen toxicity of *Rhizopus cultures* isolated from starters made by solid state fermentation. Zhonghua Min Guo Wei Sheng Wu Ji Mian Yi Xue Za Zhi. 1991;24: 229–39.
48. Weusthuis RA, Visser W, Pronk JT, Scheffers WA, van Dijken JP. Effects of oxygen limitation on sugar metabolism in yeasts: a continuous-culture study of the Kluyver effect. Microbiology. 1994;140 Pt 4: 703–15.
49. Gu S, Xu Q, Huang H, Li S. Alternative respiration and fumaric acid production of *Rhizopus oryzae*. Appl Microbiol Biotechnol. 2014;98: 5145–52.
50. Vanlerberghe GC. Alternative oxidase: a mitochondrial respiratory pathway to maintain metabolic and signaling homeostasis during abiotic and biotic stress in plants. Int J Mol Sci. Multidisciplinary Digital Publishing Institute; 2013;14: 6805–47.
51. Johnson MA, Vidoni S, Durigon R, Pearce SF, Rorbach J, He J, et al. Amino acid starvation has opposite effects on mitochondrial and cytosolic protein synthesis. PLoS One. Public Library of Science; 2014;9: e93597.

PeerJ Preprints | https://doi.org/10.7287/peerj.preprints.2742v1 | CC BY 4.0 Open Access | rec: 23 Jan 2017, publ: 23 Jan 2017